Contents lists available at ScienceDirect

Nano Energy

journal homepage: http://ees.elsevier.com

Communication

$Li_7La_3Zr_2O_{12}$ sheet-based framework for high-performance lithium–sulfur hybrid quasi-solid battery

Ayman A. AbdelHamid, Jian Liang Cheong, Jackie Y. Ying *

NanoBio Lab, 31 Biopolis Way, The Nanos, 138669, Singapore

ARTICLE INFO

Keywords
Hybrid quasi-solid electrolytes
Lithium-sulfur batteries
Garnet
$Li_7La_3Zr_2O_{12}$
Sheets

ABSTRACT

Applications of lithium batteries are challenged by their unsatisfactory safety profiles. Solid-state batteries present a very promising solution to overcome the safety issues, but their performance requires major improvement. Hybrid quasi-solid electrolyte (HQSE), comprising solid and liquid components, has emerged as a practical compromise for safer and high-performance Li batteries. Li–S system is one of the most promising Li battery candidates; however, the performance of Li–S hybrid quasi-solid battery still needs to be further enhanced. Herein, a new HQSE design comprising $Li_7La_3Zr_2O_{12}$ sheet-based solid framework imbibed with liquid electrolyte is applied to Li–S battery. The liquid-infused 3D architecture allows fast Li ion mobility and low interfacial resistance. It is also compatible with Li metal, highly processable, unleakable, and thermally stable. These attributes result in a high-performance Li–S hybrid quasi-solid system with a very good safety profile. The novel HQSE design also demonstrates improved anodic stability, which is very promising for high-voltage cathodes. The excellent performance, enhanced safety, and broad applicability of our sheet-based LLZO HQSE set the path for applications in other types of Li batteries to achieve both safe and high-performance energy storage systems.

1. Introduction

Lithium batteries are the most promising energy storage systems so far. However, their current performance is not satisfactory for demanding applications, such as electric vehicles and grid storage [1]. Safety is one of the main challenges facing the progress of lithium batteries, mainly due to the use of flammable, leakable and unstable liquid organic electrolytes [2,3], in addition to the chemical instability of Li metal anode [3–5] and thermal and mechanical instability of polymeric separators [2,6]. High-performance all-solid-state battery system has become the ultimate goal of Li battery research due to its superior safety profile [3,7]. However, solid-state electrolytes (SSEs) have limited ionic conductivity [7], and poor electrode/electrolyte interface [4], which result in high resistance and low performance. Hybrid quasi-solid electrolytes (HQSEs) have recently emerged as a practical compromise for safer and high-performance Li batteries. They typically involve 2 components: a solid component and a liquid component. The hybrid quasi-solid system benefits from the advantages associated with the solid electrolyte, while mitigating its limitations using the liquid component [4].

Lithium-sulfur (Li–S) battery is one of the most attractive Li battery systems due to the abundance, low cost and high specific capacity (1675 mAh g^{-1}) of sulfur [8–10]. However, Li–S system is still susceptible to the abovementioned safety issues, in addition to polysulfide (PS) shuttling that results in Li metal anode corrosion and active material loss [11,12]. Solid-state systems, such as P_2S_5–Li_2S [13–15], $Li_{3.25}Ge_{0.25}P_{0.75}S_4$ [16] and $Li_{10}GeP_2S_{12}$ [17], have been studied for safer and PS shuttling-free Li–S batteries. However, these systems showed limited capacity and rate capability due to the limited ionic conductivity and high interfacial resistance of the SSEs. HQSEs using $Li_{1+x}Al_xTi_{2-x}(PO_4)_3$ [10,18], $Li_{1+x}Y_xZr_{2-x}(PO_4)_3$ [11], $Li_{1.5}Al_{0.5}Ge_{1.5}(PO_4)_3$ [19–21], pristine/doped $Li_7La_3Zr_2O_{12}$ (LLZO) [12,22–25] and $LiCoO_2$ [8] exhibited an improved performance, but they were still limited by the Li ion diffusion bottleneck introduced by the solid electrolyte pellet/layer utilized. Reengineering Li–S hybrid quasi-solid system by controlling the solid component microstructure could help to overcome its current limitations. This proposition was supported by the recently published study by Qu et al. [26], whereby porous $Li_{6.4}La_3Zr_{1.4}Ta_{0.6}O_{12}$ achieved remarkably good Li–S hybrid battery performance. However, the porous solid electrolyte used in this study was fabricated using typical solid-state synthesis, which is energy-demanding (requiring 2 calcination steps at 900 °C and 1200 °C), labor-intensive (involving ball milling, calcination, mixing, pressing and sintering), and time-consuming (requiring ~3 days). In addition, ceramic electrolyte pellets are known to be brittle and susceptible to cracking during processing [27,28], especially when they are porous [29]. Further improvement in Li–S HQSE can be achieved by controlling the solid component's microstructure via more facile synthesis and robust design.

Herein, we report a HQSE design with controlled microstructure for Li–S hybrid quasi-solid battery. The HQSE consists of a 3-dimensional (3D) LLZO sheet-based solid framework imbibed with liquid electrolyte, bis(trifluoromethane)sulfonimide lithium salt (LiTFSI) in a mixture of dimethoxyethane (DME) and 1,3-dioxolane (DOL). LLZO was chosen as the solid framework due to its high ionic conductivity (cubic phase), and good chemical and electro-

* Corresponding author.
E-mail address: jyying@nbl.a-star.edu.sg (J.Y. Ying)

chemical stability [30,31]. LLZO was synthesized as sheets via a "cupcake" method, which involved a one-step sol-gel process with sucrose as a complexing and structure-directing agent. To the best of our knowledge, this is the first report of the synthesis of LLZO sheets, and also the first sol-gel method generating sheet morphology using sucrose as a structure-directing agent. The LLZO sheets were processed into a non-rigid solid framework using polytetrafluoroethylene (PTFE). The solid framework could easily absorb the liquid electrolyte due to its porous nature. In addition, its non-rigid structure allowed very good contact with electrodes, and prevented cracking during handling and battery assembly. The HQSE demonstrated high Li ion conductivity, excellent compatibility with Li metal anode, impressive thermal stability, and superior Li–S battery performance. A remarkable rate capability (~515 and ~340 mAh g^{-1} at 1 and 2C, respectively) was achieved at a loading density of 1.5 mg cm^{-2}. This rate performance is among the highest achieved by Li–S hybrid quasi-solid batteries. The 3D sheet-based framework was found to be critical for optimal battery performance. Moreover, the Li–S hybrid quasi-solid system demonstrated outstanding stability under extreme temperatures. These results illustrated the advantage of the LLZO sheet morphology, and the high potential of our 3D sheet-based structure as a HQSE framework.

2. Materials and methods

2.1. Synthesis of LLZO sheets

LLZO sheets were synthesized via the "cupcake" method. Sucrose was mixed with stoichiometric amounts of $LiNO_3$, $La(NO_3)_3{\cdot}6H_2O$, and $ZrO(NO_3)_2{\cdot}xH_2O$ (x was calculated based on the product's certificate of analysis supplied by the manufacturer) in deionized water. The sol was heated to form a brown "cupcake", and then calcined to form LLZO sheets.

2.2. Preparation of LLZO HQSE solid framework

LLZO sheets were mixed with PTFE, and rolled into a membrane, which was cut into 16.2 mm-diameter discs. The discs were dried in an oven at 60 °C.

2.3. Preparation of G/S cathode

G/S composite was synthesized according to an earlier report [32], with some modifications (Supplementary Data). G/S composite, acetylene black (AB) and vapor grown carbon fibers (VGCF) were mixed (at a weight ratio of 7:1.5:1.5) using PTFE as a binder. The mixture was rolled into a membrane, which was cut into 12.7 mm-diameter discs. The discs were dried in an oven at 60 °C.

2.4. Characterization

Morphological and structural characterizations were conducted using field emission scanning electron microscopy (FESEM) (JEOL, JSM-7400F) and transmission electron microscopy (TEM) (FEI Tecnai F20), both fitted with energy dispersive X-ray spectroscopy (EDX) (OXFORD). LLZO crystal structure was analyzed by X-ray diffraction (XRD) (Bruker D8 ADVANCE). S content in G/S composite was determined by thermal gravimetric analysis (TGA) (TGA 55, TA Instruments).

2.5. Electrochemical measurements

CR2032 coin cells were assembled inside an Ar-filled glove box with O_2 and H_2O levels of $<$ 1 ppm. Li metal was used as the anode, LLZO solid framework or commercial Celgard 2500 membrane were employed as the separator, and G/S disc was used as the cathode. 1 M LiTFSI in DME:DOL (1:1 by volume) and 2 wt% $LiNO_3$ was used as liquid electrolyte at 35–40 μL/mg sulfur. Cyclic voltammetry (CV) (0.05 mV s^{-1}) and electrochemical impedance spectroscopy (EIS) (100 kHz–10 mHz, 10 mV amplitude) measurements were performed using AUTOLAB PGSTAT302 N potentiostat. Ionic conductivity was calculated according to Equation (1) [33]:

$$\sigma = L/RA \quad (1)$$

where σ is conductivity in mS cm^{-1}, L is thickness in cm, R is resistance in mΩ, and A is surface area in cm^2. Li plating-stripping and galvanostatic discharge-charge measurements were conducted using LAND CT2001A battery cycler.

3. Results and discussion

3.1. LLZO sheets

The "cupcake" method allowed large-scale synthesis of cubic LLZO with controlled sheet morphology at a moderate temperature, as low as 850 °C, and in a short duration of ~17 h. Sol-gel approach was adopted because it enabled mixing of the precursors at the molecular level, leading to lower temperature processing, smaller grain size, and controlled morphology [34,35]. Although sol-gel synthesis of LLZO has been reported previously [31,36–38], it was typically employed to produce fine powder at less extreme conditions, as compared to solid-state synthesis, and not for synthesizing LLZO with controlled morphology. In addition, sucrose was not previously employed in LLZO synthesis, nor was it reported for inorganic sheet formation.

The synthesis process is depicted in Fig. 1a and b. Metal nitrates and sucrose were dissolved in deionized water, forming a clear solution at a pH of 1.5. Sucrose acted as a polydentate ligand that bound the metal ions to form homogeneous metal ion-sucrose complex solution [39]. When the solution was heated, sucrose underwent polymerization, followed by foaming due to thermal decomposition [39–41]. Subsequently, a brown "cupcake" was formed whereby the internal structure was composed of large sheets (Fig. 1c). Upon further heating, the organic component was decomposed and oxidized as CO_2 and H_2O gases, while the homogeneously distributed metal ions reacted and crystallized into LLZO, which adopted the sheet morphology of the precursor (Fig. 1d). In the absence of sucrose, only bulk LLZO was obtained (Fig. S1a), illustrating the critical role played by sucrose in sheet structure formation. The sheets have micron-sized lateral dimensions, typically $>$ 10 μm, while their thickness is in the nanometer range, ~190 nm (Fig. 1e). Junctions, which probably formed by coalescence during calcination, connected the sheets to each other (Fig. S2). The resulting continuous Li ion pathways would facilitate Li ion conductivity [42]. Powder XRD analysis (Fig. 1g) showed that the precursor sheets were amorphous. The LLZO sheets crystallized into the cubic phase (JCPDS #01-080-4947), and matched the cubic phase of commercial nano Al-doped LLZO particles in XRD pattern. The LLZO crystallite size was calculated to be 49.5 nm using the Scherrer's equation (based on the highest intensity plane (420)). High-resolution TEM imaging showed an interplanar d-spacing of 0.326 nm, which corresponded to the (400) plane of cubic LLZO (Fig. 1f). EDX showed the uniform distribution of elements over the sheets (Fig. 1h–k).

3.2. LLZO HQSE

LLZO HQSE was constructed using LLZO sheets as building blocks for the 3D solid framework, and LiTFSI in DME/DOL as the liquid component. The 3D sheet-based framework readily imbibed the liquid electrolyte, and the HQSE showed fast Li ion diffusion, excellent compatibility with Li metal, and high mechanical, thermal and anodic stability. Fig. 2a presents the schematic of LLZO HQSE preparation. The interconnected LLZO sheets were bound together using PTFE, and then processed into ~250 μm-thick discs (Fig. 2b: inset), which were imbibed with the liquid electrolyte. The LLZO sheets were assembled together as a 3D framework with a porous nature (Fig. 2b–d). The LLZO framework could easily imbibe the liquid electrolyte, providing superior electrolyte infiltration, as compared to commercial Celgard 2500 membrane, which has limited porosity (Fig. 2e). LLZO HQSE displayed excellent thermal stability, with no shrinkage or morphological change, after exposure to 150 °C for 10 min (Fig. 2f). This was due to the high thermal stability of LLZO and PTFE binder [43]. In contrast, the Celgard membrane melted under the testing condi-

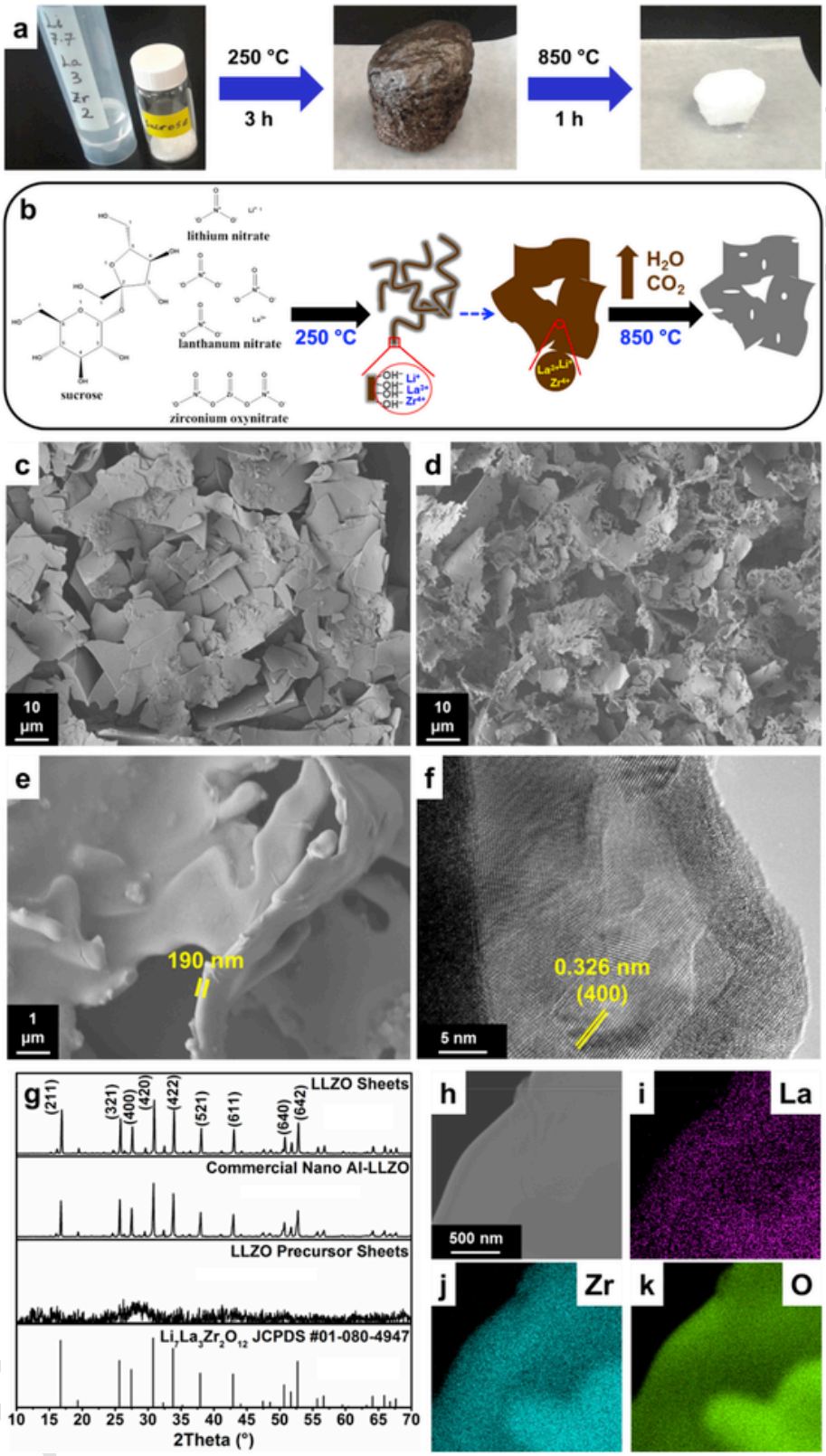

Fig. 1. (a) Photographs and (b) schematic depiciting the synthesis of LLZO sheets. (c–e) FESEM images, (f) TEM image, (g) XRD patterns, (h) scanning TEM image, and (i–k) EDX elemental maps of (c–f, h–k) LLZO sheets and (g) LLZO precursor sheets and LLZO sheets.

of LLZO HQSE was investigated via EIS at room temperature. The Nyquist plot (Fig. 2g) showed a straight line, whose intercept with the real axis indicated bulk resistance [33]. No semi-circle was observed, indicating the absence of grain boundary resistance, which was attributed to the infiltration of the liquid electrolyte within the LLZO framework. The ionic conductivity of LLZO HQSE was calculated to be 0.7 mS cm^{-1}, which was comparable to that obtained using Celgard separator (Fig. 2h), showing the suitability of LLZO HQSE for utilization in lithium batteries. Stability of LLZO HQSE against

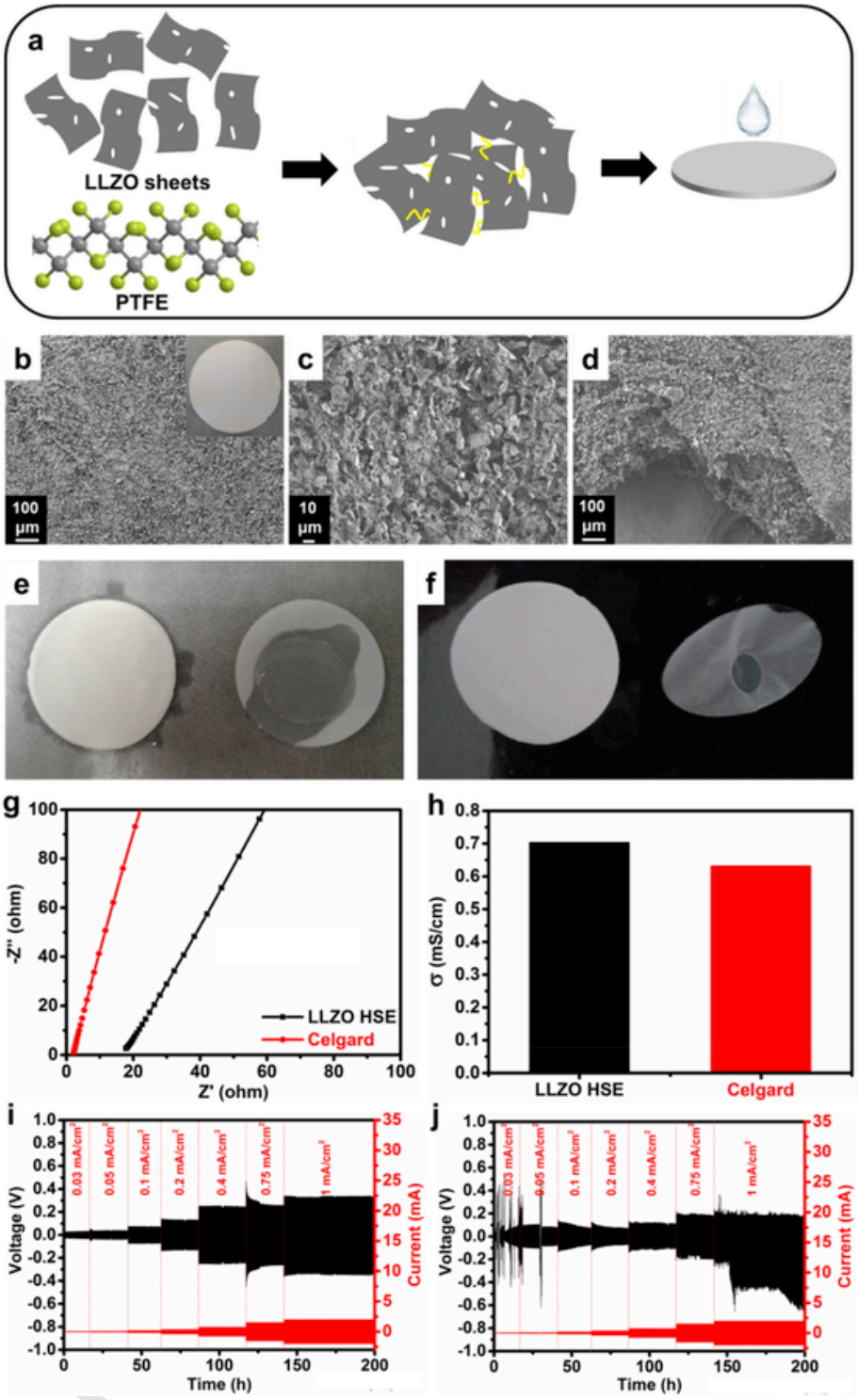

Fig. 2. (a) Schematic depicting LLZO HQSE preparation. (b–d) FESEM images and (inset in b) photograph of LLZO HQSE solid framework. (e) Electrolyte imbibition test, (f) thermal stability test, (g) Nyquits plots, and (h) ionic conductivity of LLZO HQSE (left in e, f) and Celgard (right in e, f). Li symmetric cell cycling of (i) LLZO HQSE and (j) Celgard. Liquid electrolyte volume was 50 μL for elelctrolyte imbibition and thermal stability tests, and 30 μL for ionic conductivity and Li symmetric cell cycling tests.

Li metal was studied by galvanostatic cycling of a symmetric Li/LLZO HQSE/Li cell for 200 h at increasing current densities (Fig. 2i). LLZO HQSE displayed smooth cycling with no significant voltage fluctuation. In contrast, the Celgard separator displayed significant instability during initial cycling, and major hysteresis at the high current density of 1 mA cm^{-2} (Fig. 2j). These results demonstrated that the LLZO HQSE has a more stable interface with Li metal, resulting in uniform Li deposition and mitigating dendrite growth [6]. LLZO HQSE also exhibited good mechanical stability; its non-rigid structure could tolerate processing during preparation and cell assembly/disassembly, with no cracking or disintegration (Fig. S3). Moreover, LLZO HQSE showed enhanced anodic stability (Fig. S4), rendering it a promising candidate for utilization with high-voltage cathodes.

3.3. Li–S hybrid quasi-solid battery

LLZO HQSE was applied in Li–S hybrid quasi-solid system, displaying high electrochemical reversibility and enhanced battery performance. A current collector-free cathode was prepared using graphene (G)/S composite, carbon additives and PTFE binder. The carbon additives provided the necessary electrical links within the G/S composite, while PTFE enabled the processing into a flexible free-standing electrode (Fig. 3a). CV and EIS of Li–S hybrid quasi-solid battery showed high electrochemical reversibility and reduced polarization over cycling (Figs. S5a and b), which indicated good electrode/electrolyte contact. Li–S battery using Celgard showed higher polarization and charge-transfer resistance, as shown by CV and EIS analyses, respectively (Figs. S5c and d). This indicated that LLZO HQSE had better contact with the electrode than Celgard, which resulted in less polarization and charge-transfer resistance. This could be explained by the soft nature of the free-standing electrode and LLZO HQSE, which were prepared in a similar manner using PTFE as a binder. This helped both membranes to stick together after assembly, resulting in better contact with each other. Li–S battery with LLZO HQSE has an initial capacity of 1448.3 mAh g^{-1} at 0.1C, which was higher than the 1405.0 mAh g^{-1} achieved with Celgard membrane (Fig. 3d). After 10 cycles, their capacities reached 957.2 and 874.2 mAh g^{-1}, respectively. This showed that LLZO HQSE could stabilize the Li–S battery system, resulting in improved performance.

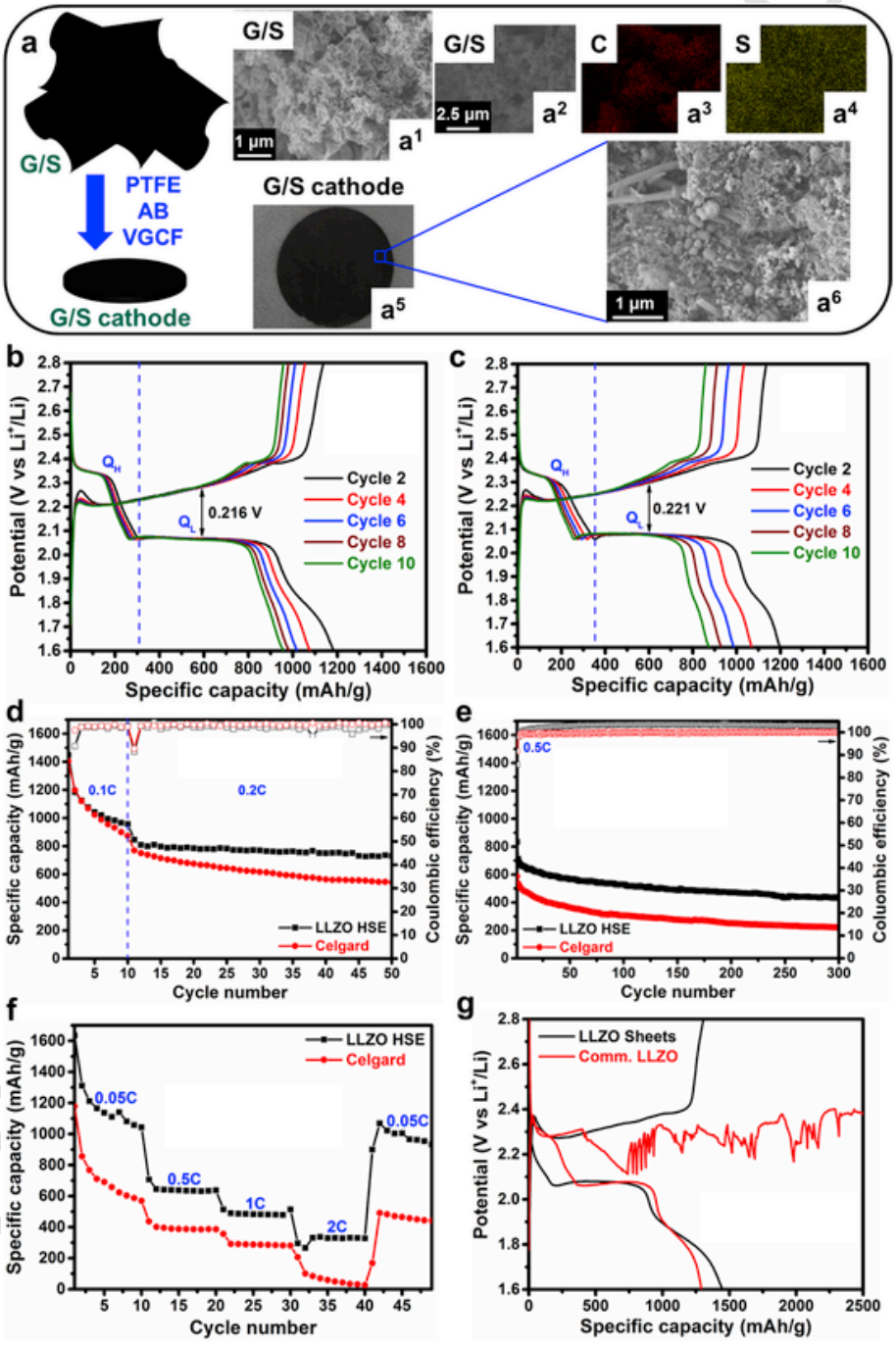

Fig. 3. (a) Schematic (left) depicting G/S cathode preparation. (a^1, a^2) FESEM images and (a^3, a^4) EDX elemental maps of G/S composite. (a^5) Photograph and (a^6) FESEM image of G/S cathode. (b, c) Discharge-charge profiles, (d, e) cycling performance, (f) rate capability, and (g) initial discharge-charge profiles of (b, d–g) LLZO HQSE, (c–f) Celgard, and (g) commercial LLZO HQSE.

Discharge-charge profiles were studied to gain further insight into the Li–S hybrid quasi-solid battery performance. LLZO HQSE displayed two distinct discharge plateaus and two overlapping charge plateaus (Fig. 3b), which was consistent with the CV profile, and similar to that displayed by Celgard membrane (Fig. 3c). However, LLZO HQSE showed a lower polarization of 0.216 V, as compared to 0.221 V shown by Celgard, which indicated enhanced redox kinetics and better energy efficiency [9], further confirming the minimized electrode/electrolyte interfacial resistance due to the good contact in the former. The higher cycling stability shown by LLZO HQSE could be understood by studying the discharge plateaus carefully. The upper plateau capacity (Q_H) loss was ~50% less with LLZO HQSE, as compared to Celgard. (Fig. S6). The significantly reduced Q_H loss by LLZO HQSE indicated its effective role in mitigating PS diffusion [9,44], resulting in less active material loss, which reduced the lower plateau capacity (Q_L) and total capacity (Q_T) loss. PS shuttling control by LLZO was reported previously, and was attributed to its chemical affinity to soluble PS [12,26], and the physical barrier introduced by the LLZO framework [26]. On the other hand, Celgard displayed high Q_H loss due to its inability to control PS shuttling, which resulted in increased Q_L and Q_T fading.

The improved performance of LLZO HQSE could be better observed with prolonged cycling. LLZO HQSE retained 730.7 mAh g^{-1} when cycled for another 40 cycles at 0.2C, with capacity retention (after the first cycle) of 90.2% and capacity fade/cycle (after the first cycle) of 0.25%, as compared to 542.9 mAh g^{-1}, 72.3% and 0.71% shown by Celgard, respectively (Fig. 3d). At 0.5C, LLZO and Celgard have initial capacities of 834.5 and 586.8 mAh g^{-1}, which decreased to 431.5 and 220.7 mAh g^{-1} after 300 cycles, with capacity retention (after the first cycle) of 60.5% and 41.1%, and capacity fade/cycle (after the first cycle) of 0.13% and 0.2%, respectively (Fig. 3e). Analysis of the discharge-charge profiles at 0.5C agreed with that of 0.1C profiles. A smaller polarization of 0.349 V was observed with LLZO HQSE, as compared to 0.57 V with Celgard (Figs. S7a and b), indicating better reaction kinetics, which agreed with the results mentioned above. Interestingly, LLZO HQSE also showed ~50% less Q_H loss, as compared to Celgard, which resulted in lower Q_L and Q_T loss (Figs. S7c and d), leading to better capacity retention. This confirmed our earlier conclusion about the role of LLZO in controlling PS shuttling.

The cycled LLZO HQSE appeared as an orange-colored semi-solid disc with no separate liquid electrolyte observed (Fig. S8a). This showed that the liquid electrolyte was completely imbibed within the LLZO solid framework, and that the battery operated in a hybrid quasi-solid state with no risk of electrolyte leakage. The orange color could be due to the PS anchored to the LLZO sheets [26]. On the other hand, the battery operated using Celgard showed a brown-colored liquid (Fig. S8b), implying substantial PS diffusion, which could explain its inferior performance. In order to rule out the role of thickness in enhancing the cycling performance and minimizing PS shuttling, we conducted another control experiment using 10 pieces of Celgard membrane to match the thickness of the LLZO membrane (~250 μm). It was observed that the performance of the battery with 10 pieces of Celgard was comparable to that with only 1 piece, and significantly less than that of LLZO HQSE (Fig. S8c). This confirmed that both the composition and structure of LLZO HQSE gave a better electrochemical performance with lower PS shuttle, as compared to Celgard. These results also agreed with the better electrolyte infiltration of LLZO membrane forming a quasi-solid electrolyte, as compared to the slow and incomplete electrolyte imbibition of the 10 stacked Celgard layers (Fig. S9).

Interestingly, the sheet-like morphology of the cycled LLZO and its cubic crystal structure were stable after cycling (Figs. S10a and b), indicating its stability against the liquid electrolyte and PS, which agreed with previous results [12]. LLZO HQSE was further tested at higher current densities to investigate its rate capability, which is the main limitation for Li–S hybrid quasi-solid systems. LLZO HQSE showed capacities of 1635.0, 707.1, 514.5 and 331.1 mAh g^{-1} at 0.05C, 0.5C, 1C and 2C, respectively, and could recover to 1068.7 mAh g^{-1} at 0.05C. On the other hand, Celgard showed significantly inferior performance of 1179.2, 401.1, 291.5, 100.5 mAh g^{-1} at 0.05C, 0.5C, 1C and 2C, respectively, and only recovered to 490.8 mAh/g at 0.05C (Fig. 3f). The enhanced LLZO HQSE performance as compared to Celgard agreed with the results mentioned above, thus confirming the capability of LLZO HQSE to stabilize the cycling performance of Li–S battery. The Li–S hybrid quasi-solid battery performance was among the best reported in the literature (Table S1). This could be attributed to the intricate LLZO HQSE design. Unlike the commonly used dense solid pellets/layers, the interconnected LLZO sheets formed a non-rigid 3D solid framework that was infused with liquid electrolyte. This design allowed battery operation in a hybrid quasi-solid state, while ensuring high Li ion conductivity and low interfacial resistance, thus achieving high capacity, cycling stability, and rate capability. In addition, PS shuttling was significantly reduced by the LLZO sheets and the solid framework's microstructure, which further improved battery performance. These results demonstrated the potential of our design for achieving a high-performance hybrid quasi-solid Li–S battery. Although we have used less electrolyte/sulfur (E/S) ratio than similar hybrid quasi-solid systems [26] while showing better performance, more work will be done in the future to minimize E/S ratio, targeting E/S ratio of <10.

In order to validate the significance of the 3D sheet-based framework structure for battery performance, commercial nano Al-doped cubic LLZO was used as a control. The commercial LLZO has an irregular morphology, mostly showing agglomerated bulky particles (Fig. S11a). At 0.1C, commercial LLZO HQSE showed an initial discharge capacity of 1291.2 mAh g^{-1} (Fig. 3g), which was slightly less than that achieved by our LLZO HQSE. However, the commercial LLZO HQSE was not able to follow up with the charge process, displaying a highly fluctuating charge voltage. This phenomenon has been reported recently, and was attributed to the failure to conduct Li ions [45]. Such failure could be explained by the very dense and compact structure of commercial LLZO HQSE (Fig. S11b), which could have been completely blocked by the interphase layer formed on the surface of LLZO particles [12] during the initial discharge. The large volume of liquid electrolyte observed upon disassembling the cell (Fig. S11c) also revealed the inability of the commercial LLZO HQSE to imbibe liquid electrolyte due to its compact, non-porous structure. These results illustrated the significance of the LLZO's sheet morphology and the LLZO HQSE's porous architecture for optimal battery operation.

One of the main advantages of hybrid quasi-solid systems is improved battery safety. Therefore, we conducted thermal stability experiments to evaluate the battery safety profile of LLZO HQSE. Li–S batteries were exposed to two scenarios of extreme temperature conditions. In the first scenario, the cells were heated gradually, initially at 150 °C for 30 min, and then at 180 °C and 210 °C for 10 min each. In the second scenario, the cells were exposed to a sudden high temperature of 200 °C for 5 min. LLZO HQSE was stable in both scenarios (Fig. 4a, c and d), while Celgard showed very poor stability profile. In the former scenario, the Celgard membrane was damaged, leading to full contact between both electrodes (Fig. 4b). In the second scenario, the cell exploded violently (Fig. 4e). These results demonstrated the superior safety profile of LLZO HQSE-based Li–S battery, and highlighted the potential role of hybrid quasi-solid electrolytes in substantially improving the safety profile of lithium batteries.

4. Conclusion

A novel methodology has been developed for the synthesis of LLZO sheets, which were used as building blocks for the construction of a 3D LLZO framework that was imbibed with liquid electrolyte, forming a high-performance HQSE. The LLZO HQSE eliminated electrolyte leakage problem, ensured adequate contact with electrodes, and enhanced stability against Li metal anode. In addition, it allowed fast Li ion mobility and superior stability at high temperatures, as compared to commercial polymeric separators. These excellent properties were reflected in the Li–S hybrid quasi-solid battery performance, which was among the best reported so far, with high capacity, prolonged stability, excellent rate capability, and enhanced thermal stability.

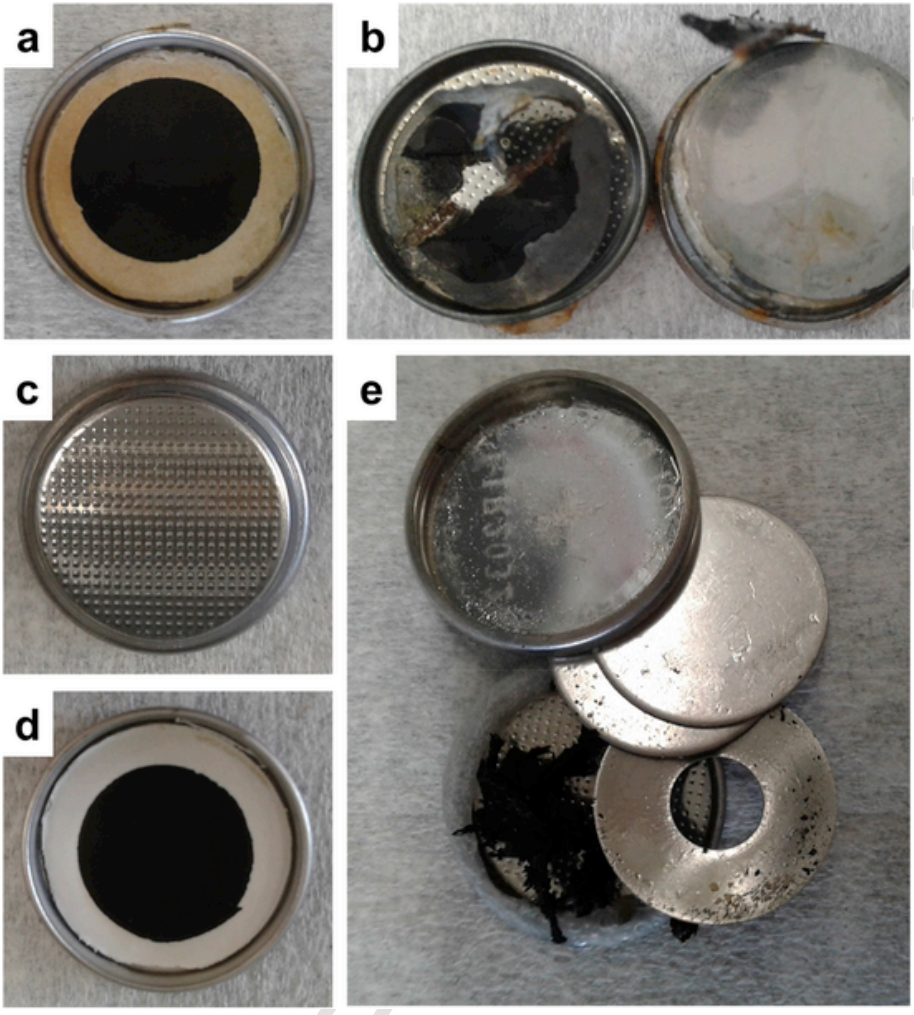

Fig. 4. Disassembled Li–S batteries produced with (a) LLZO HQSE, and (b) Celgard after thermal stability test (first scenario). (c, d) Li–S hybrid quasi-solid battery after thermal stability test (second scenario): (c) before and (d) after cell disassembly. (e) Li–S battery produced with Celgard after cell explosion from thermal stability test (second scenario).

CRediT authorship contribution statement

Ayman A. AbdelHamid: Conceptualization, Methodology, Investigation, Writing - original draft. **Jian Liang Cheong:** Methodology, Writing - review & editing. **Jackie Y. Ying:** Conceptualization, Writing - review & editing, Supervision.

Declaration of competing interest

The authors declare that they have no known competing financial interests or personal relationships that could have appeared to influence the work reported in this paper.

Acknowledgements

The authors thank Dr. Jinhua Yang of NBL for helpful discussions, and Yiming Li of NBL for his assistance with some experiments. This work was funded by NBL (Biomedical Research Council, Agency for Science, Technology and Research, Singapore).

Appendix A. Supplementary data

Supplementary data to this article can be found online at https://doi.org/10.1016/j.nanoen.2020.104633.

References

[1] Y. Sun, N. Liu, Y. Cui, Nat. Energy 1 (2016) 16071.
[2] H.W. Kim, P. Manikandan, Y.J. Lim, J.H. Kim, S. Nam, Y. Kim, J. Mater. Chem. 4 (2016) 17025–17032.
[3] Y. Meesala, A. Jena, H. Chang, R.-S. Liu, ACS Energy Lett 2 (2017) 2734–2751.
[4] M. Keller, A. Varzi, S. Passerini, J. Power Sources 392 (2018) 206–225.
[5] J. Zhang, Y. Bai, X.-G. Sun, Y. Li, B. Guo, J. Chen, G.M. Veith, D.K. Hensley, M.P. Paranthaman, J.B. Goodenough, S. Dai, Nano Lett. 15 (2015) 3398–3402.
[6] D. Zhou, R. Liu, Y.-B. He, F. Li, M. Liu, B. Li, Q.-H. Yang, Q. Cai, F. Kang, Adv. Energy Mater. 6 (2016) 1502214.
[7] R. Chen, W. Qu, X. Guo, L. Li, F. Wu, Mater. Horiz. 3 (2016) 487–516.
[8] D. Moy, S.R. Narayanan, J. Electrochem. Soc. 164 (2017) A560–A566.
[9] L. Luo, A. Manthiram, ACS Energy Lett 2 (2017) 2205–2211.
[10] X. Yu, A. Manthiram, Adv. Funct. Mater. 29 (2019) 1805996.
[11] X. Yu, Z. Bi, F. Zhao, A. Manthiram, Adv. Energy Mater. 6 (2016) 1601392.
[12] K.K. Fu, Y. Gong, S. Xu, Y. Zhu, Y. Li, J. Dai, C. Wang, B. Liu, G. Pastel, H. Xie, Y. Yao, Y. Mo, E. Wachsman, L. Hu, Chem. Mater. 29 (2017) 8037–8041.
[13] M. Agostini, Y. Aihara, T. Yamada, B. Scrosati, J. Hassoun, Solid State Ionics 244 (2013) 48–51.
[14] T. Yamada, S. Ito, R. Omoda, T. Watanabe, Y. Aihara, M. Agostini, U. Ulissi, J. Hassoun, B. Scrosati, J. Electrochem. Soc. 162 (2015) A646–A651.
[15] Y. Zhang, T. Liu, Q. Zhang, X. Zhang, S. Wang, X. Wang, L. Li, L.-Z. Fan, C.-W. Nan, Y. Shen, J. Mater. Chem. 6 (2018) 23345–23356.
[16] M. Nagao, Y. Imade, H. Narisawa, T. Kobayashi, R. Watanabe, T. Yokoi, T. Tatsumi, R. Kanno, J. Power Sources 222 (2013) 237–242.
[17] X. Yao, N. Huang, F. Han, Q. Zhang, H. Wan, J.P. Mwizerwa, C. Wang, X. Xu, Adv. Energy Mater. 7 (2017) 1602923.
[18] X. Yu, Z. Bi, F. Zhao, A. Manthiram, ACS Appl. Mater. Interfaces 7 (2015) 16625–16631.
[19] Q. Wang, J. Guo, T. Wu, J. Jin, J. Yang, Z. Wen, Solid State Ionics 300 (2017) 67–72.
[20] X. Wu, J. Zong, H. Xu, W. Wang, X. Liu, RSC Adv. 6 (2016) 57346–57356.
[21] Q. Wang, J. Jin, X. Wu, G. Ma, J. Yang, Z. Wen, Phys. Chem. Chem. Phys. 16 (2014) 21225–21229.

[22] K. Fu, Y. Gong, G.T. Hitz, D.W. McOwen, Y. Li, S. Xu, Y. Wen, L. Zhang, C. Wang, G. Pastel, J. Dai, B. Liu, H. Xie, Y. Yao, E.D. Wachsman, L. Hu, Energy Environ. Sci. 10 (2017) 1568–1575.
[23] X. Huang, C. Liu, Y. Lu, T. Xiu, J. Jin, M.E. Badding, Z. Wen, J. Power Sources 382 (2018) 190–197.
[24] M.M.U. Din, R. Murugan, Electrochem. Commun. 93 (2018) 109–113.
[25] X. Chen, T. Wang, W. Lu, T. Cao, M. Xue, B. Li, C. Zhang, J. Alloys Compd. 744 (2018) 386–394.
[26] H. Qu, J. Ju, B. Chen, N. Xue, H. Du, X. Han, J. Zhang, G. Xu, Z. Yu, X. Wang, G. Cui, J. Mater. Chem. 6 (2018) 23720–23729.
[27] K.M. Diederichsen, E.J. McShane, B.D. McCloskey, ACS Energy Lett 2 (2017) 2563–2575.
[28] J. Zheng, Y.-Y. Hu, ACS Appl. Mater. Interfaces 10 (2018) 4113–4120.
[29] J. Fan, T. Lin, F. Hu, Y. Yu, M. Ibrahim, R. Zheng, S. Huang, J. Ma, Ceram. Int. 43 (2017) 3647–3653.
[30] Z.D. Gordon, T. Yang, G.B. Gomes Morgado, C.K. Chan, ACS Sustain. Chem. Eng. 4 (2016) 6391–6398.
[31] J. Li, Z. Liu, W. Ma, H. Dong, K. Zhang, R. Wang, J. Power Sources 412 (2019) 189–196.
[32] G. Zhou, L.-C. Yin, D.-W. Wang, L. Li, S. Pei, I.R. Gentle, F. Li, H.-M. Cheng, ACS Nano 7 (2013) 5367–5375.
[33] Y. Zhu, F. Wang, L. Liu, S. Xiao, Z. Chang, Y. Wu, Energy Environ. Sci. 6 (2013) 618–624.
[34] V. Aravindan, K. Karthikeyan, S. Ravi, S. Amaresh, W.S. Kim, Y.S. Lee, J. Mater. Chem. 20 (2010) 7340.
[35] Y.X. Gao, X.P. Wang, W.G. Wang, Q.F. Fang, Solid State Ionics 181 (2010) 33–36.
[36] N. Janani, S. Ramakumar, L. Dhivya, C. Deviannapoorani, K. Saranya, R. Murugan, Ionics 17 (2011) 575.
[37] Y. Shimonishi, A. Toda, T. Zhang, A. Hirano, N. Imanishi, O. Yamamoto, Y. Takeda, Solid State Ionics 183 (2011) 48–53.
[38] A.A. Hubaud, D.J. Schroeder, B. Key, B.J. Ingram, F. Dogan, J.T. Vaughey, J. Mater. Chem. 1 (2013) 8813–8818.
[39] R.N. Das, A. Bandyopadhyay, S. Bose, J. Am. Ceram. Soc. 84 (2001) 2421–2423.
[40] S. Bose, S.K. Saha, J. Am. Ceram. Soc. 86 (2003) 1055–1057.
[41] K. Prabhakaran, J. Joseph, N.M. Gokhale, S.C. Sharma, R. Lal, Ceram. Int. 31 (2005) 327–331.
[42] T. Yang, J. Zheng, Q. Cheng, Y.-Y. Hu, C.K. Chan, ACS Appl. Mater. Interfaces 9 (2017) 21773–21780.
[43] Y. Yuan, D. Yu, Y. Yin, B. Tang, E. Li, S. Zhang, J. Mater. Sci. Mater. Electron. 27 (2016) 13288–13293.
[44] S. Zhao, R. Fang, Z. Sun, S. Wang, J.-P. Veder, M. Saunders, H.-M. Cheng, C. Liu, S.P. Jiang, F. Li, Small Methods 2 (2018) 1800067.
[45] Q. Pang, A. Shyamsunder, B. Narayanan, C.Y. Kwok, L.A. Curtiss, L.F. Nazar, Nat. Energy 3 (2018) 783–791.

Biography

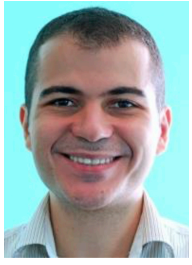

Ayman A. AbdelHamid is a Research Scientist at NanoBio Lab, Singapore. He received his M.Sc. in Nanoscience and Technology from Nile University, Egypt in 2012, and his Ph.D. in Materials Science and Engineering from Nanyang Technological University, Singapore in 2017. His research interests include development of nanomaterials and nanocomposites for energy storage applications.

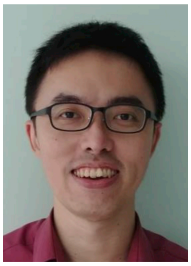

Jian Liang Cheong is a Senior Lab Officer at the NanoBio Lab, Singapore. He received his B.Sc. (Honours) in Chemistry from the National University of Singapore, Singapore in 2010. Currently, he is doing his Ph.D. under the supervision of Prof. Jackie Ying. He is interested in developing practical and scalable systems for energy storage.

Jackie Y. Ying received her B.E. and Ph.D. from The Cooper Union and Princeton University, respectively. She joined the faculty at Massachusetts Institute of Technology in 1992, where she was Professor of Chemical Engineering until 2005. She was the Founding Executive Director of the Institute of Bioengineering and Nanotechnology in Singapore from 2003 to 2018. Prof. Ying currently leads the NanoBio Lab as A*STAR Senior Fellow. For her research on nanostructured materials, Prof. Ying has been recognized with the American Ceramic Society Ross C. Purdy Award, David and Lucile Packard Fellowship, Office of Naval Research Young Investigator Award, National Science Foundation Young Investigator Award, Camille Dreyfus Teacher-Scholar Award, American Chemical Society Faculty Fellowship Award in Solid-State Chemistry, Technology Review's Inaugural TR100 Young Innovator Award, American Institute of Chemical Engineers (AIChE) Allan P. Colburn Award, International Union of Biochemistry and Molecular Biology Jubilee Medal, Materials Research Society Fellowship, Royal Society of Chemistry Fellowship, Crown Prince Grand Prize in the Brunei Creative, Innovative Product and Technological Advancement (CIPTA) Award, American Institute for Medical and Biological Engineering Fellowship, Academy of Sciences of Iran Medal of Honor, American Association for the Advancement of Science Fellowship, Singapore National Academy of Science Fellowship, and Turkish Academy of Sciences Academy Prize in Science and Engineering Sciences. Prof. Ying was elected a World Economic Forum Young Global Leader, and inducted to the German National Academy of Sciences, Leopoldina and the U.S. National Academy of Inventors. She was named one of the "One Hundred Engineers of the Modern Era" by AIChE in its Centennial Celebration, and a Highly Cited Researcher (Cross-Field Category) by Clarivate Analytics. She was the inaugural winner of the Mustafa Prize "Top Scientific Achievement Award" in 2015 for her research in bio-nanotechnology.